Electronic Supplementary Material (ESI) for Physical Chemistry Chemical Physics.

Detailed insights into the formation pathway of CdS and ZnS in solution: a multi-modal *in situ* characterization approach

J. Ströh,[a] T. Hess,[a] L. Ohrt,[a] H. Fritzsch,[a] M. Etter,[b] A.-C. Dippel,[b] L. D. Nyamen[a, c,*] and H. Terraschke [a,*]

[a] Institut für Anorganische Chemie, Christian-Albrechts-Universität zu Kiel, Max-Eyth-Str. 2, 24118 Kiel, Germany. E-mail: hterraschke@ac.uni-kiel.de.

[b] DESY Photon Science, Notkestr. 85, 22607 Hamburg, Germany.

[c] Department of Inorganic Chemistry, University of Yaoundé I, P. O. Box 812, Yaoundé, Cameroon.

Table of contents

1 Overview on previous *in situ* studies during synthesis of CdS and ZnS particles

Table S1: List of *in situ* measurements performed during different syntheses of CdS and ZnS particles.

Compound	*In situ* characterization method	Synthesis method	Reference
CdS	Small-angle X-ray scattering (SAXS) and wide-angle X-ray scattering (WAXS) analysis	Two-step nucleation and growth of CdS nanoparticles in aqueous solution	Schiener *et al.*[1]
CdS	UV/Vis absorption spectroscopy	Synthesis in AOT (Cadmium Dioctylsulfosuccinate) reverse micelles	Petit *et al.*[2]
CdS	UV/Vis absorption spectroscopy	Synthesis in Cadmium Bis(ethyl-2-hexyl) sulfosuccinate reverse micelles	Motte *et al.*[3]
CdS	UV/Vis absorption spectroscopy	Decomposition of sodium thiosulfate by γ-radiation	Yin *et al.*[4]
CdS nanowires	Fluorescence spectroscopy	Pulsed-laser deposition (PLD) on interdigitated Au-electrodes (IDE)	An *et al.*[5]
CdS NPs	Thermogravimetric analysis (TGA) and differential scanning calorimetry (DSC)	Thermolysis of Cadmium dodecanethiolate dispersed in the polymer P3HT	Borriello *et al.*[6]
Gold NPs on silica-coated CdSe-Dot / CdS-Rot nanocrystals	UV/Vis absorption spectroscopy	Ultrasound-assisted *in situ* growth	Tang *et al.*[7]
CdSe / $Cd_xZn_{1-x}S$ NPs	UV/Vis absorption spectroscopy	*In situ* interface alloying	Boldt *et al.*[8]
ZnS adsorbent	*In situ* Raman spectrum analysis	sulfidation calcination	Xie *et al.*[9]
ZnS nanowires	*In situ* heating transmission electron microscopy (TEM)	Metal-organic chemical vapor deposition	Kim *et al.*[10]
ZnS NPs	*In situ* small angle X-ray scattering (SAXS) and X-ray absorption spectroscopy (XAS)	Metal salt and thioacetamide dissolved in water	Meneau *et al.*[11]

Table S2: Experimental conditions for monitoring the formation of CdS and ZnS using the *in situ* setups A (University of Kiel), B (DESY, up to 120 °C), and C (DESY, up to 180 °C). Abbreviations: Exp. = experiment; SSP = single-source precursor; conc. = concentration; add. = addition; vol. = volume; sol. = solution; EG = ethylene glycol; temp. = temperature.

Exp. number	Setup	PETRA III beamline	X-ray energy / keV	Temp. / °C	λ_{ex} /nm	Reactor EG vol. / mL	Manual add. (SSP) / mmol	Vol. SSP sol. / mL	Conc. SSP sol. / mol/L	Manual add. (Acetate) / mmol	Manual add. (Thiourea) / mmol
I	A	-	-	100	375	30	-	-	-	-	-
II	A	-	-	100	375	30	-	5	0.1	-	-
III	A	-	-	100	375	30	-	5	0.5	-	-
IV	A	-	-	100	375	30	0.9	-	-	-	-
V	A	-	-	100	390	40	-	-	-	41 (Cd)	37
VI	A	-	-	80	365	40	-	-	-	41 (Cd)	37
VII	A	-	-	25	365	40	-	-	-	41 (Cd)	37
VIII	B	P02.1	60	100	365	40	-	-	-	41 (Cd)	37
IX	B	P21.1	103	100	340	40	-	-	-	41 (Cd)	37
X	A	-	-	100	390	25	-	-	-	26 (Cd)	23
XI	A	-	-	100	340	25	-	-	-	8 (Zn)	9
XII	A	-	-	100	340	25	-	-	-	26 (Zn)	23
XIII	A	-	-	100	-	10	-	-	-	10 (Zn)	12
XIV	B	P02.1	60	100	365	40	-	-	-	20 (Zn)	20
XV	C	P02.1	60	180	-	4	-	-	-	2 (Zn)	2

2 Experimental part

2.1 In situ measurement setups

2.2.1 Setup A

This setup comprised an EasyMax® 102 stationary workstation (Mettler Toledo, Gießen, Germany) and a Fluorolog 3 spectrometer (Horiba, Jovin Yvon GmbH, Unterhaching, Germany) equipped with an iHR-320-FA triple-grating imaging spectrograph, a Syncerity charge-coupled device (CCD) detector, and a 450 W Xe lamp. The spectrometer and reactor were connected using a Y-shaped optical fibre, which transferred the excitation light to the reactor and the luminescence emitted by the product to the spectrometer. The EasyMax® 102 workstation allowed automatic and precise control of the stirring conditions, temperature, and solution doses.
The (in situ) obtained emission spectra were additionally used for calculating the respective colour coordinates, which were plotted at the Commission internationale de l'éclairage (CIE) 1931 diagram. In principle, the colour coordinates are determined through a mathematical combination between the wavelength and intensity of the emitted light with the sensitivity of the human eyes to this respective wavelength, in order to obtain colour matching and visual equivalence between measured spectral functions and real sensed colours, as reported in detail by Shevell at al. [12]

2.2.2 Setup B

To achieve the shortest pathway of the X-ray beam through the reaction mixture, a modified glass reactor containing an inserted glass tube was used, as previously described. [13] Herein, the reactor content was analysed using the P02.1 and P21.1 beamlines at the PETRA III storage ring of the Deutsches Elektronen-Synchrotron, (DESY). The reactor holder comprised an integrated stirring and heating system; [14] moreover, it featured X-ray entering and exiting openings and a perpendicular opening to allow illumination with a light source for simultaneous *in situ* light transmission measurements. A portable EPP2000 spectrometer (StellarNet Inc., Tampa, FL, United States) equipped with a CCD-based detector was used to record optical spectra every 30 s. The spectrometer was connected to an optical fibre submerged in the reactant mixture. During the light transmission experiments, product formation in solution was identified by the increase in solution turbidity and decrease in the intensity of the detected light source (340 and 365 nm LED, Sahlmann Photochemical Solutions, Bad Segeberg, Germany) through the reaction solution. An automatic dosing system (Titrando 902, Metrohm AG, Filderstadt, Germany) was used to add the solutions to the reactor. The XRD and total scattering patterns were recorded every 10 s at the P02.1 beamline (60 keV, λ = 0.20721 Å) and every 30 s at the P21.1 beamline (103 keV, λ = 0.12090 Å), respectively. Both beamlines were fitted with 2D detectors (model XRD1621, PerkinElmer, USA). The data were analysed using the DawnDiamond and DESY data helper software. The total scattering data were converted into PDFs using the xPDFsuite software. [17] The XRD and total scattering data were normalised to compensate for the changes in beam intensity; furthermore, for the sake of clarity, the background caused by the reactor walls and solvent was eliminated.

2.2.3 Setup C

Setup C comprised a synchrotron-based reaction cell for the analysis of chemical reactions (SynRAC) reactor.[15, 16] Herein, this reactor was used to investigate the fabrication of ZnS NPs at high temperatures, such as 180 °C, which was not possible using setups A and B. The SynRAC reactor comprised an Al casing that accommodated borosilicate reaction vessels (V_{max} = 5 mL). The Al casing was surrounded by a mantle of Cu-galvanised heating wires, which was used to heat the samples to the target

temperature. The reaction cell was mounted in the transmission geometry. The synchrotron X-ray beams penetrated the cell at the centre of the vessel 50 mm above the ground plate. The Al casing was thinned to 100 µm in this area to ensure minimal beam intensity loss.

2.2 *Ex situ* measurements

A Stadi-p XRD instrument (Cu Kα1 radiation, λ = 1.540598 Å, equipped with a Ge monochromator and a Mythen 1k detector) (STOE, Germany) was used for the *ex situ* XRD measurements. Reflection spectra were recorded at 25 °C using a Varian Techtron Pty UV–Vis–NIR two-channel Cary 5000 spectrometer (Agilent Technologies, USA), using $BaSO_4$ as the reference material.

3 Supplementary results

3.1 Synthesis of the single-source precursor

Within preliminary experiments, the formation of the synthesized [$CdC_2H_8N_4S_2Cl_2$] precursor was initially confirmed using XRD and IR spectroscopy. The powder XRD pattern of the fabricated SSP (Fig. S1a†) matched the simulated pattern of [$CdC_2H_8N_4S_2Cl_2$]. [17] The absence of additional reflections indicated that the obtained compound was pure. The IR spectrum of the synthesised SSP presented bands corresponding to different features of the [$CdC_2H_8N_4S_2Cl_2$] complex (Fig. S1b†), such as the bands at 3385 and 3280 cm^{-1} (primary NH_2 stretching), 3193 cm^{-1} (thioamide stretching), 1612 cm^{-1} (primary NH_2 deformation), 1394 cm^{-1} (C–N, valence), and 1098 cm^{-1} (C–N stretching). [18]

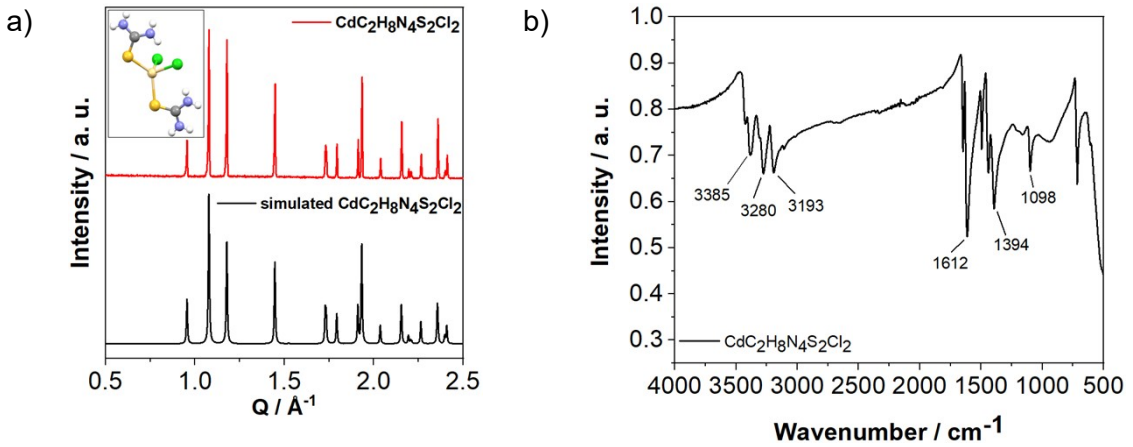

Figure S1: a) Comparison between measured and simulated [17] powder diffraction patterns for the dichlorobis(thiourea)cadmium(II) ($CdC_2H_8N_4S_2Cl_2$) single-source precursor. Inset: Structure of the single-source precursor (Cd = peach, Cl = green, S = dark yellow, C = grey, N = blue, H = white). b) Infrared spectroscopy results for the synthesized single-source precursor $CdC_2H_8N_4S_2Cl_2$.

3.2 Influence of the solvent on *in situ* luminescence measurements

Prior to monitoring the formation of semiconductor NPs using *in situ* luminescence spectroscopy, it is necessary to ensure that the changes observed in the *in situ* emission spectra occurred because of product formation. Therefore, reference *in situ* luminescence spectra (λ_{ex} = 375 nm) were obtained. For a typical experiment, pure EG was heated to 100 °C for 2 h followed by cooling (Exp. I, Table S2†). This approximated, for instance, the conditions of Exp. II (Table S2†) for CdS synthesis. The *in situ*-recorded emission spectra of EG in the batch reactor included a weak band in the range of 400–600 nm (Fig. S2†), which was assigned to the Raman scattering effects of EG. [19] The intensity was very low during heating for 2 h and it slightly increased during cooling.

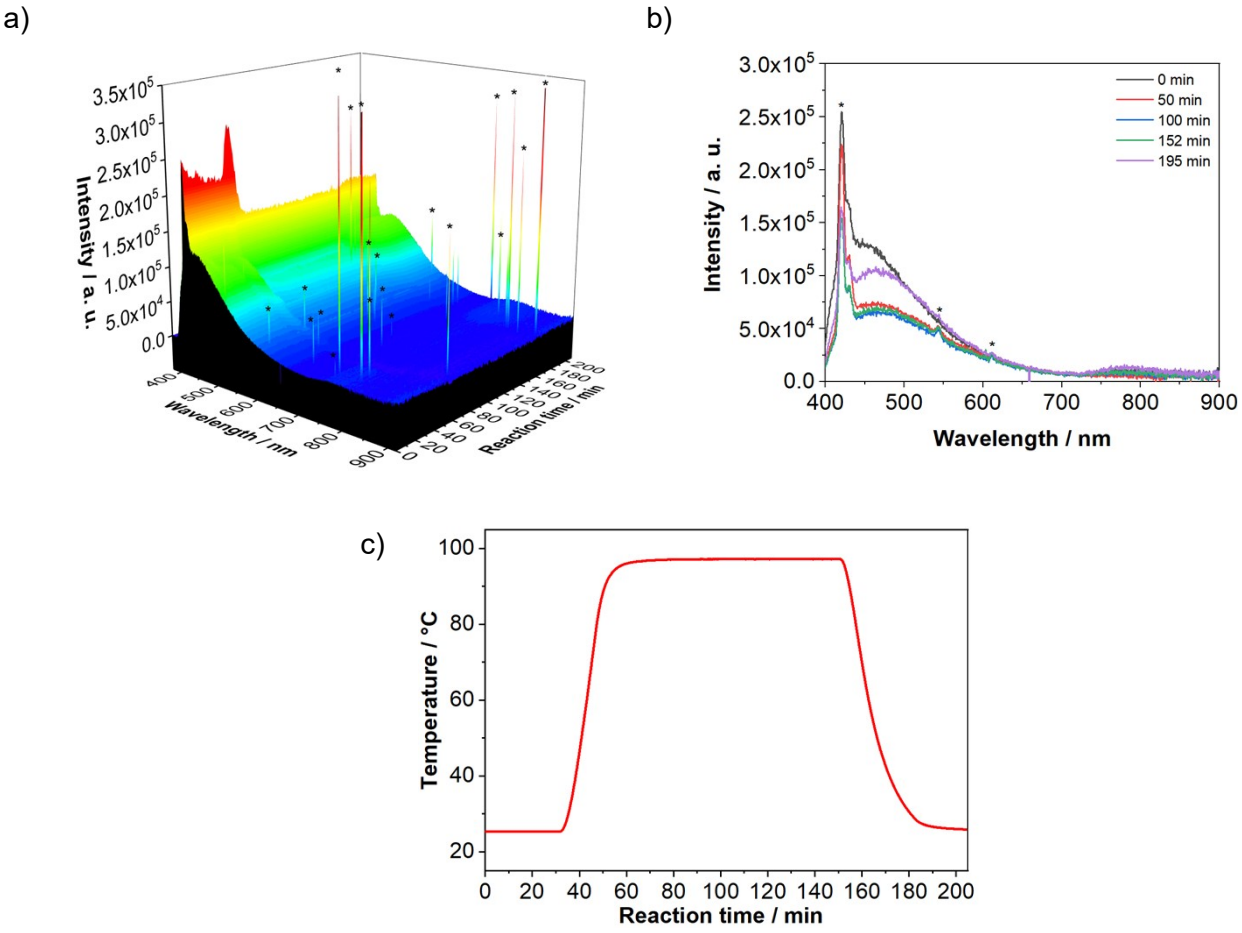

Figure S2: a) and b) Reference *in situ* 3D luminescence measurement (λ_{ex} = 375 nm) for pure ethylene glycol (Exp. I) during c) the temperature program, simulating typical conditions for the synthesis of CdS and ZnS NPs. Due to the low emission signal of the EG, the sensitivity of the detector was strongly increased in these measurements, causing the artifacts marked here by the asterisk (*) signs.

3.3 Solved SSP: Influence of the precursor concentration on the CdS formation

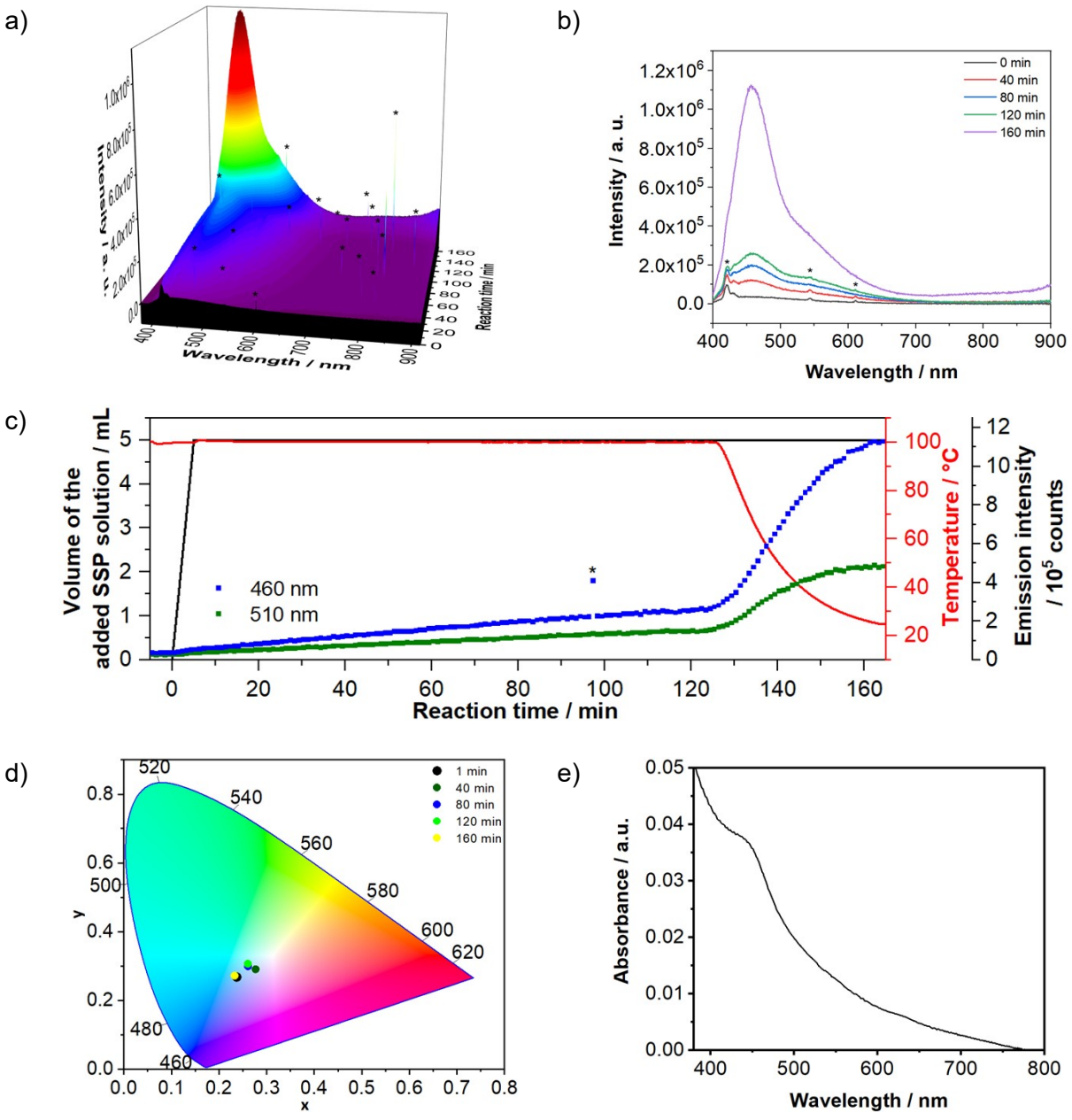

Figure S3: a) and b) *In situ* 3D luminescence measurement of the reaction of the 0.1 M SSP solution in ethylene glycol at 100 °C (λ_{ex} = 375 nm). The asterisk (*) signs mark the measurement artifacts. c) Comparison plot for the time-dependent added volume of the SSP solution, temperature and emission intensity at 460 and 510 nm. d) Commission Internationale de l'Eclairage (CIE) diagram displaying the colour changes during the reaction and e) *ex situ* absorption measurement of the product.

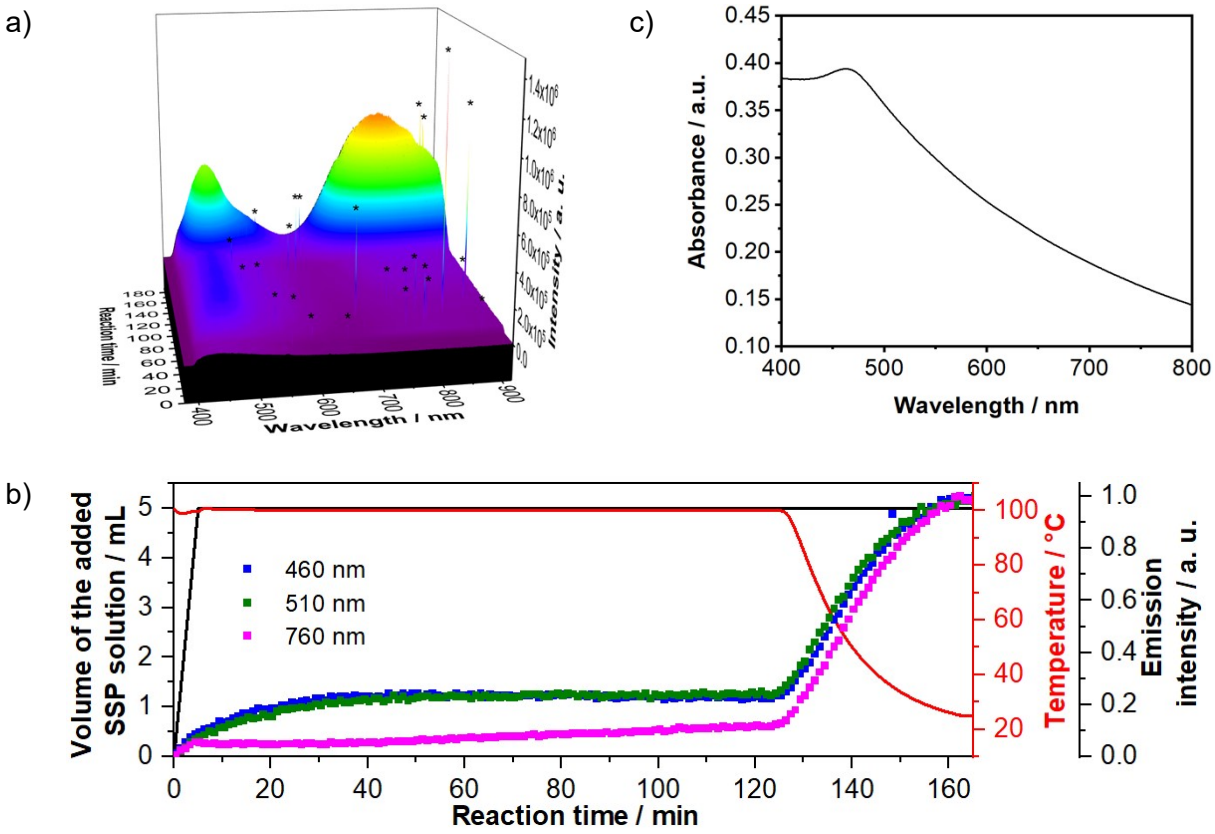

Figure S4: a) *In situ* luminescence measurement of the reaction of the 0.5 M SSP solution in ethylene glycol at 100 °C (λ_{ex} = 375 nm, Exp. III). b) Time-dependence of the added volume of the SSP solution, of the temperature and of the emission intensity at 460, 510 and 760 nm. The asterisk (*) signs mark measurement artifacts. c) *Ex situ* absorption measurement of the respective product.

3.4 Solid SSP: Influence of the temperature and the precursor concentration on the CdS formation

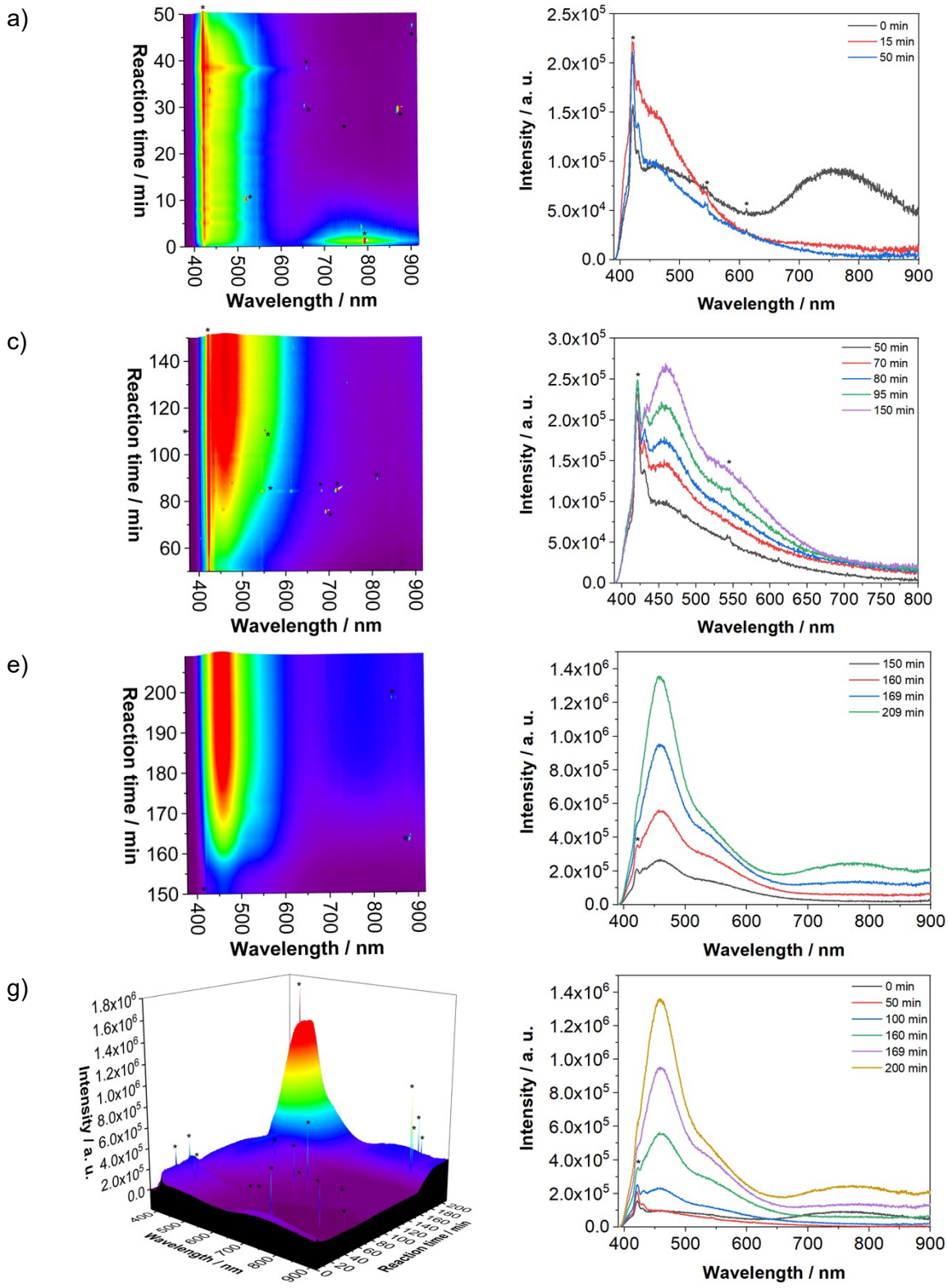

Figure S5: *In situ* luminescence measurement recorded during the reaction of the 0.9 mmol solid SSP in ethylene glycol at 100 °C (λ_{ex} = 375 nm, Exp. IV) at a) t = 0 – 50 min, b) t = 50 – 150 min, c) t = 150 – 210 min and d) complete overview. The asterisk (*) signs mark the measurement artifacts.

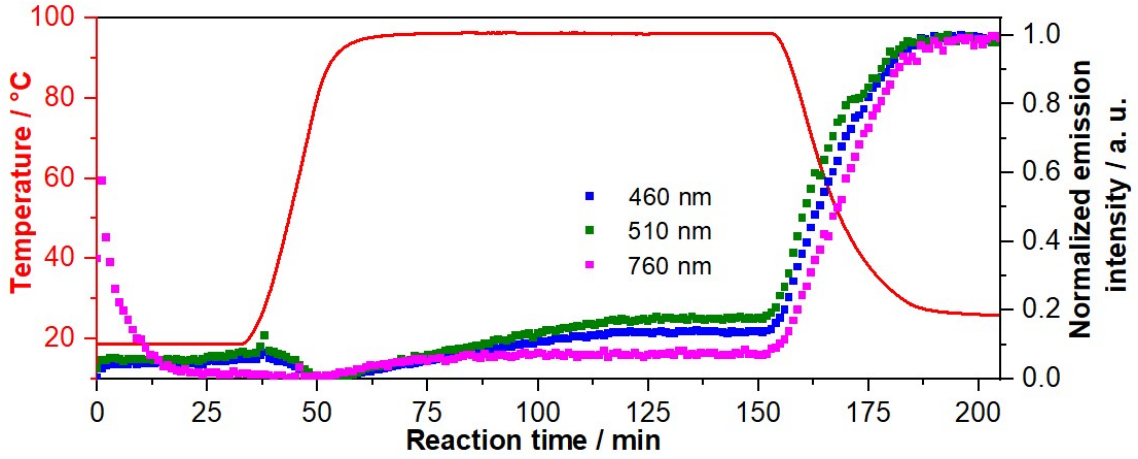

Figure S6: Time-dependent development of the reaction temperature in comparison to the intensity of different emission bands at λ_{em} = 460, 510 and 760 nm (λ_{ex} = 375 nm), (Exp. IV).

3.5 CdS synthesis using solid of cadmium acetate and thiourea

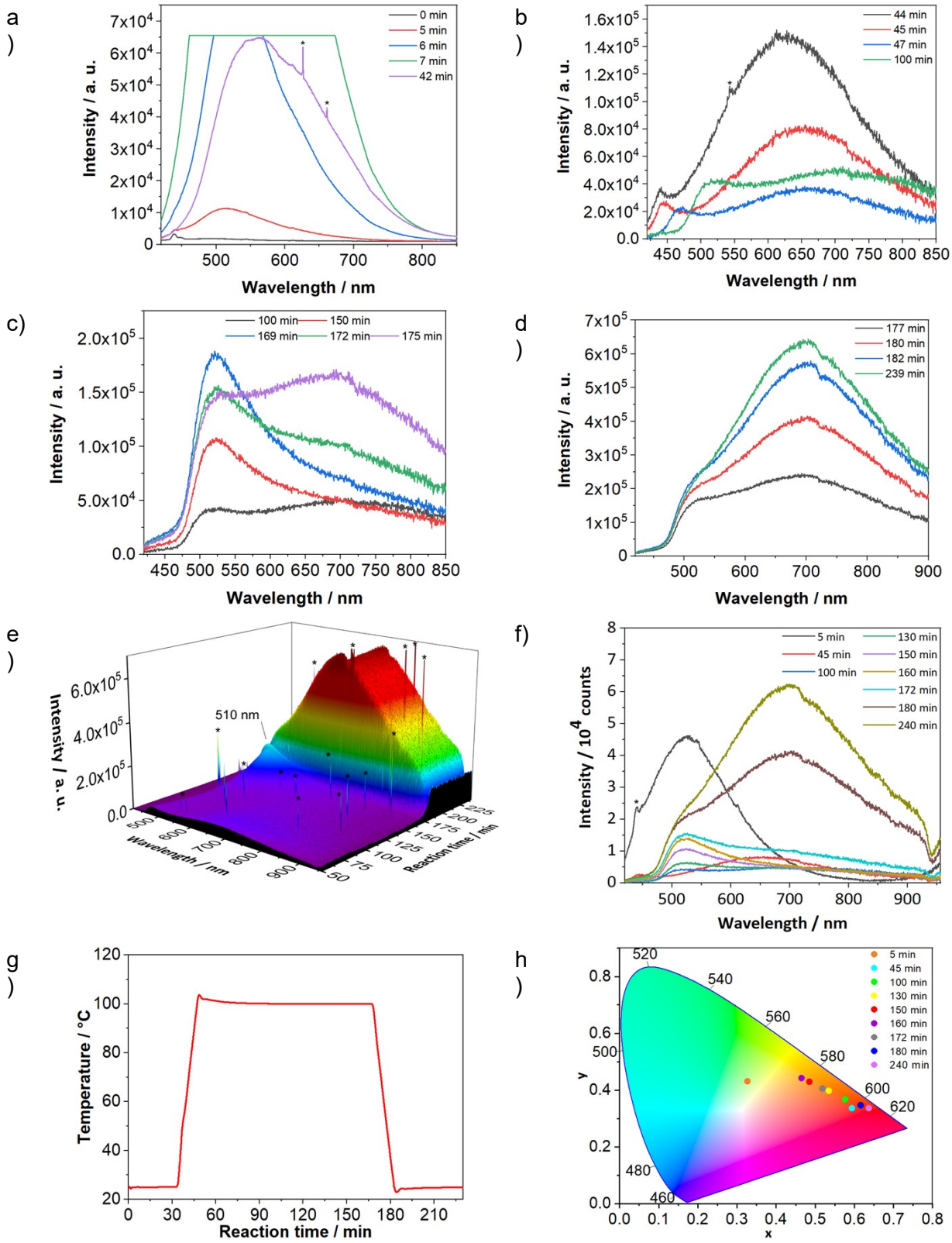

Figure S7: *In situ* luminescence measurements (λ_{ex} = 390 nm) during the CdS synthesis upon mixing solid $Cd(CH_3COO)_2 \cdot 2H_2O$ and thiourea (Exp. V), heating up to 100 °C. The experiment is divided here into discrete reaction periods (a-d) for a better understanding. e) and f) Overall overview of most important features of the respective *in situ* luminescence measurements. The asterisk (*) signs mark the measurement artifacts. g) Respective temperature program and CIE 1931 diagram displaying the time-dependent changes on emission colour.

4 Influence of the reaction temperature

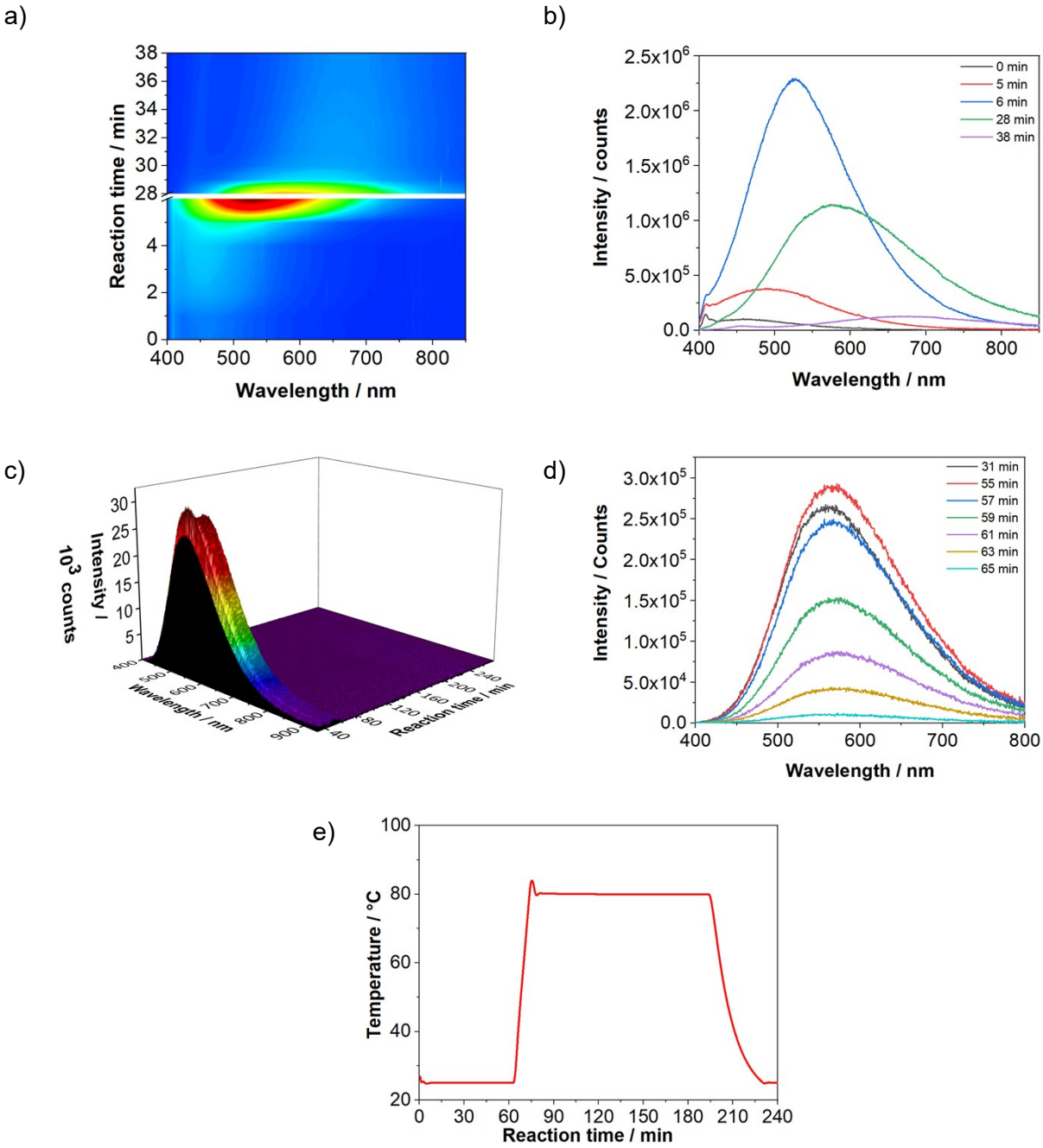

Figure S8: *In situ* luminescence measurement during the reaction between $Cd(CH_3COO)_2 \cdot 2 H_2O$ and thiourea at 80 °C (λ_{ex} = 365 nm, Exp. VI) for a) and b) t = 0 – 38 min as well as for c) and d) t = 38-245 min. e) Respective temperature program.

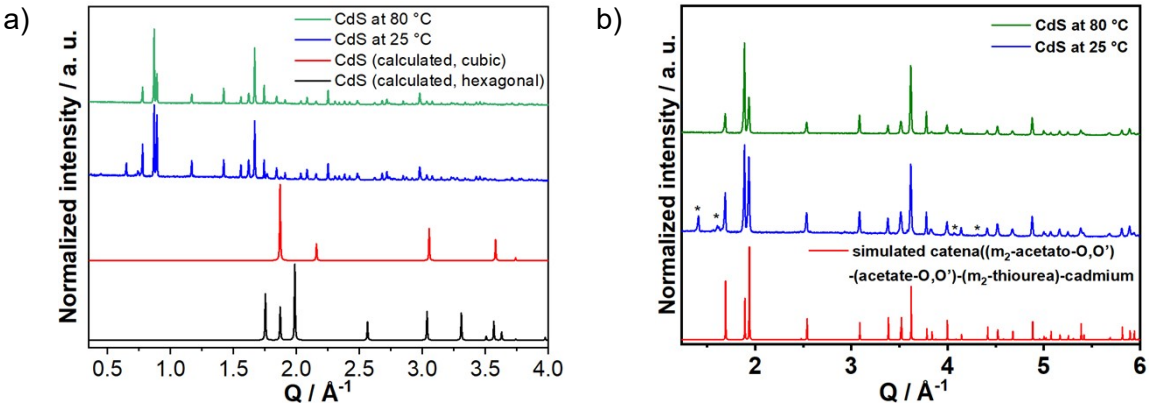

Figure S9: XRD measurement of the products of the reaction between $Cd(CH_3COO)_2 \cdot 2 H_2O$ and thiourea at 80 and 25 °C (Exps. VI and VII) compared to simulated diffraction pattern of a) cubic [20] and hexagonal [21] CdS patterns as well as with the one of the b) catena((m$_2$-acetato-O,O')-(acetate-O,O')-(m$_2$-thiourea)-cadmium complex. [22]

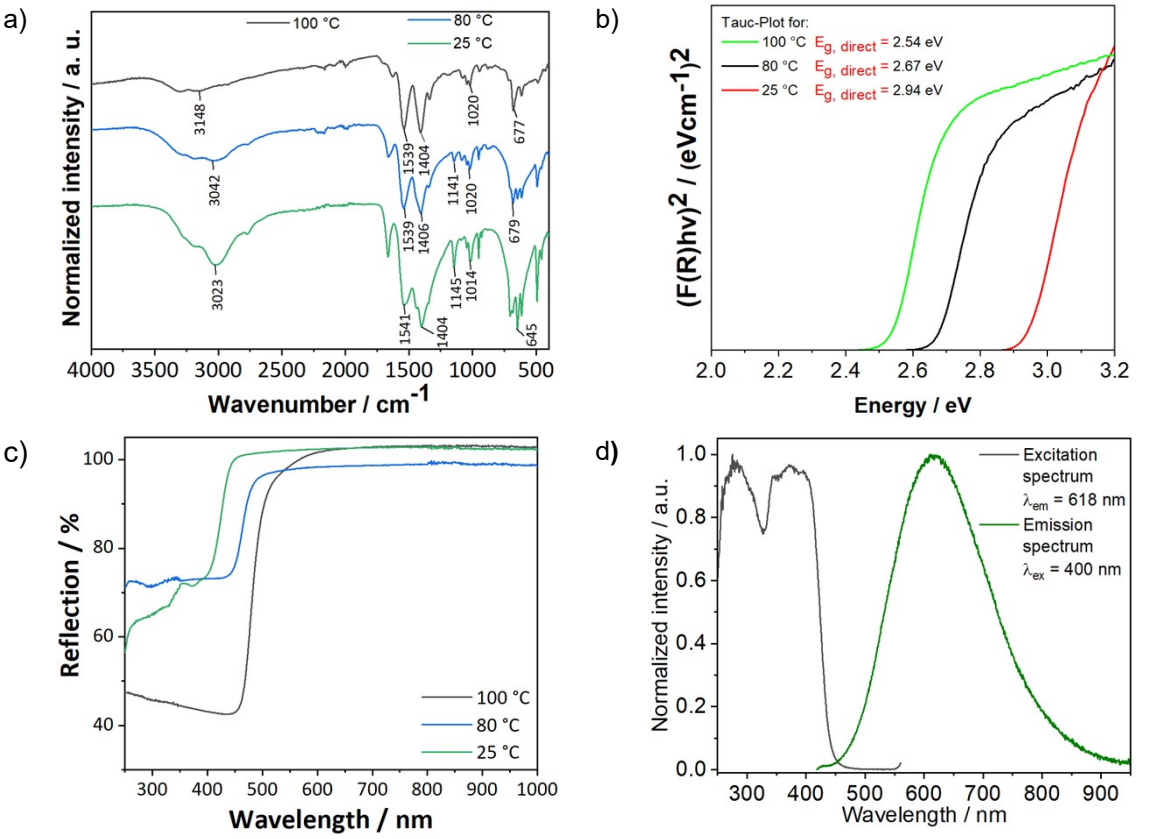

Figure S10: a) IR measurements of the products of the reaction between $Cd(CH_3COO)_2 \cdot 2 H_2O$ and thiourea at 100, 80 and 25 °C (Exps. V- VII). Respective b) Tauc-Plot and c) reflection measurements for determining the band gap of the products. d) Ex situ emission and excitation spectra of the catena((m$_2$-acetato-O,O')-(acetate-O,O')-(m$_2$-thiourea)-cadmium complex synthesized at 25 (Exp. VII).

Ex situ IR spectra collected from the dried and washed products demonstrate that the vibration bands at 3148 cm^{-1} (O–H stretching), 1539 and 1404 cm^{-1} (O–H bending), 1020 cm^{-1} (C–O stretching) and 677 cm^{-1} (C–H stretching) were observed for CdS synthesised at 100 °C. These bands match the IR spectrum of EG, [23] indicating the passivation of the CdS particle surfaces with these molecules. The additional bands at 1141 and 1145 cm^{-1} (C=S stretching) in the IR spectra of the products synthesised at 80 and 25 °C, respectively, were ascribed to the presence of thiourea-based ligands in the catena((m_2-acetato-O,O')-(acetate-O,O')-(m_2-thiourea)-cadmium) complex structure. The intensity of this band in the IR spectrum of the product synthesised at 25 °C was stronger than that in the IR spectrum of the product synthesised at 80 °C; moreover, this band was not detected in the IR spectrum of the product synthesised at 100 °C. These results indicate that upon increasing temperature, more precursor was converted and more of the product was formed. The *ex situ* UV–Vis spectra of the products were obtained and the bandgaps of the products synthesised at 100, 80, and 25 °C were 2.54, 2.67, and 2.94 eV, respectively.

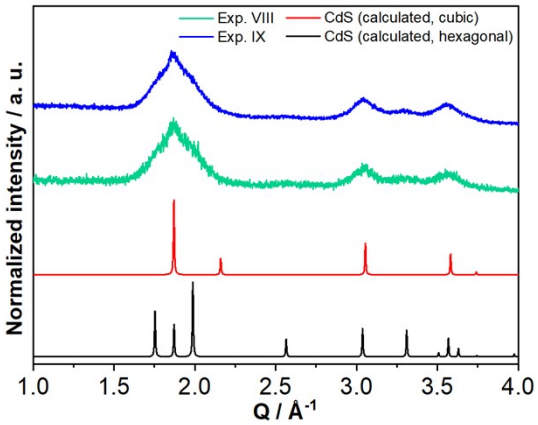

Figure S11: XRD patterns from the simulated cubic, [21] hexagonal [22] CdS in comparison to products of the reaction between $Cd(CH_3COO)_2 \cdot 2\ H_2O$ and thiourea at 100 °C, monitored by *in situ* XRD (Exp. VIII) and *in situ* total scattering (Exp. IX).

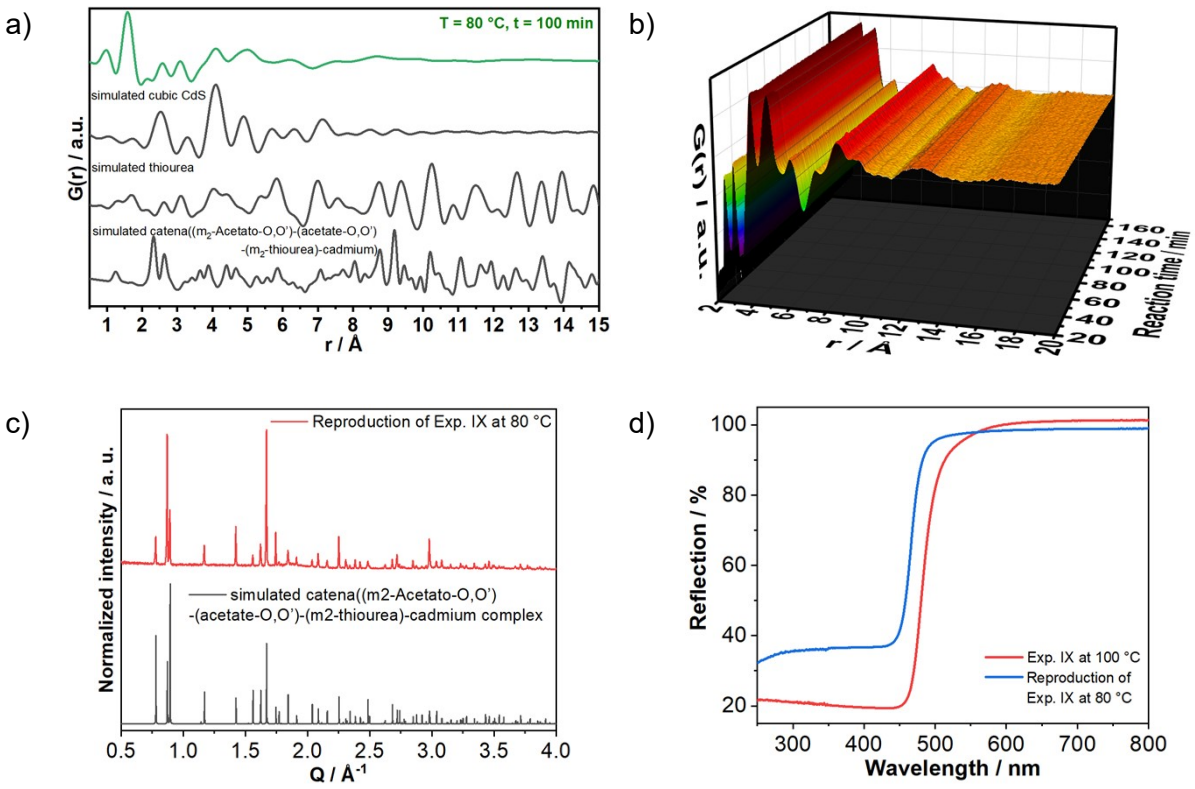

Figure S12: a) PDF patterns for different reaction times during the reaction of between $Cd(CH_3COO)_2 \cdot 2H_2O$ and thiourea at 80 °C in comparison to simulated patterns for cubic CdS, [20] catena((m$_2$-Acetato-O,O')-(acetate-O,O')-(m$_2$-thiourea)-cadmium), [22] as well as for thiourea b) respective 3D time-dependent PDF patterns. c) *Ex situ* XRD patterns from the simulated catena((m$_2$-Acetato-O,O')-(acetate-O,O')-(m$_2$-thiourea)-cadmium) [22] complex and the product of the reproduction of Exp. IX at 80 °C. d) *Ex situ* UV/Vis reflection measurements of the products synthesised at 100 °C and at 80 °C.

5 Synthesis of CdS via the addition of solid double-source precursors to preheated ethylene glycol

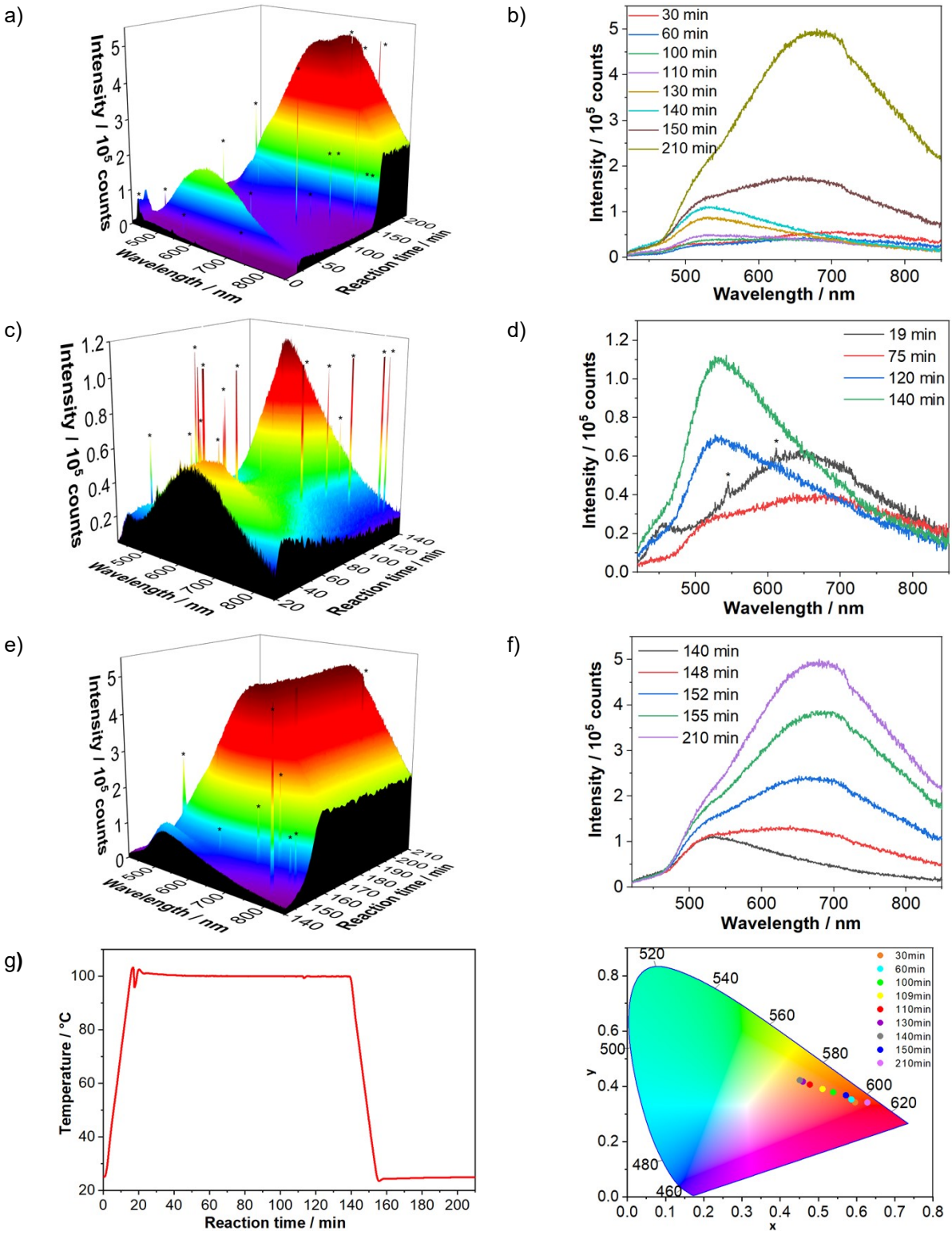

Figure S13: a) and b) *In situ* luminescence measurements recorded during the synthesis of CdS via the addition of $Cd(CH_3COO)_2 \cdot 2\ H_2O$ and thiourea to preheated EG (Exp. X). Zoom of respective *in situ* luminescence spectra for c) and d) t = 19 – 140 min as well as for e) and f) t = 140 – 210 min. The asterisk (*) signs mark the measurement artifacts. g) Respective temperature program and CIE 1931 diagram displaying the time-dependent changes on emission colour.

a)

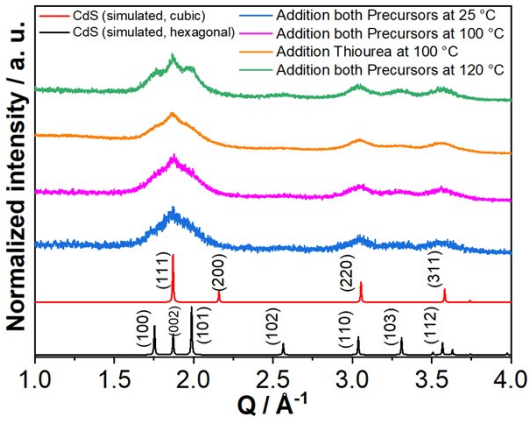

b)

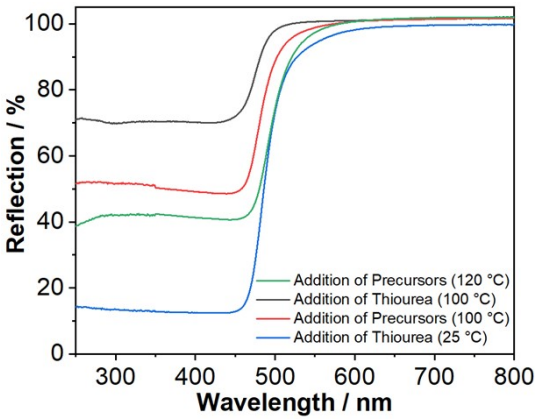

Figure S14: a) Comparison between simulated cubic [20] and hexagonal [21] CdS diffraction patterns with XRD measurements of the products obtained by the addition of solid $Cd(CH_3COO)_2 \cdot 2\ H_2O$ and thiourea precursors at 25, 100 and 120 °C as well as by the addition of thiourea to $Cd(CH_3COO)_2 \cdot 2\ H_2O$ EG solution at 100 °C. b) Respective UV/Vis reflection spectra.

6 ZnS synthesis using solid $Zn(CH_3COO)_2 \cdot 2\ H_2O$ and thiourea at 100 °C

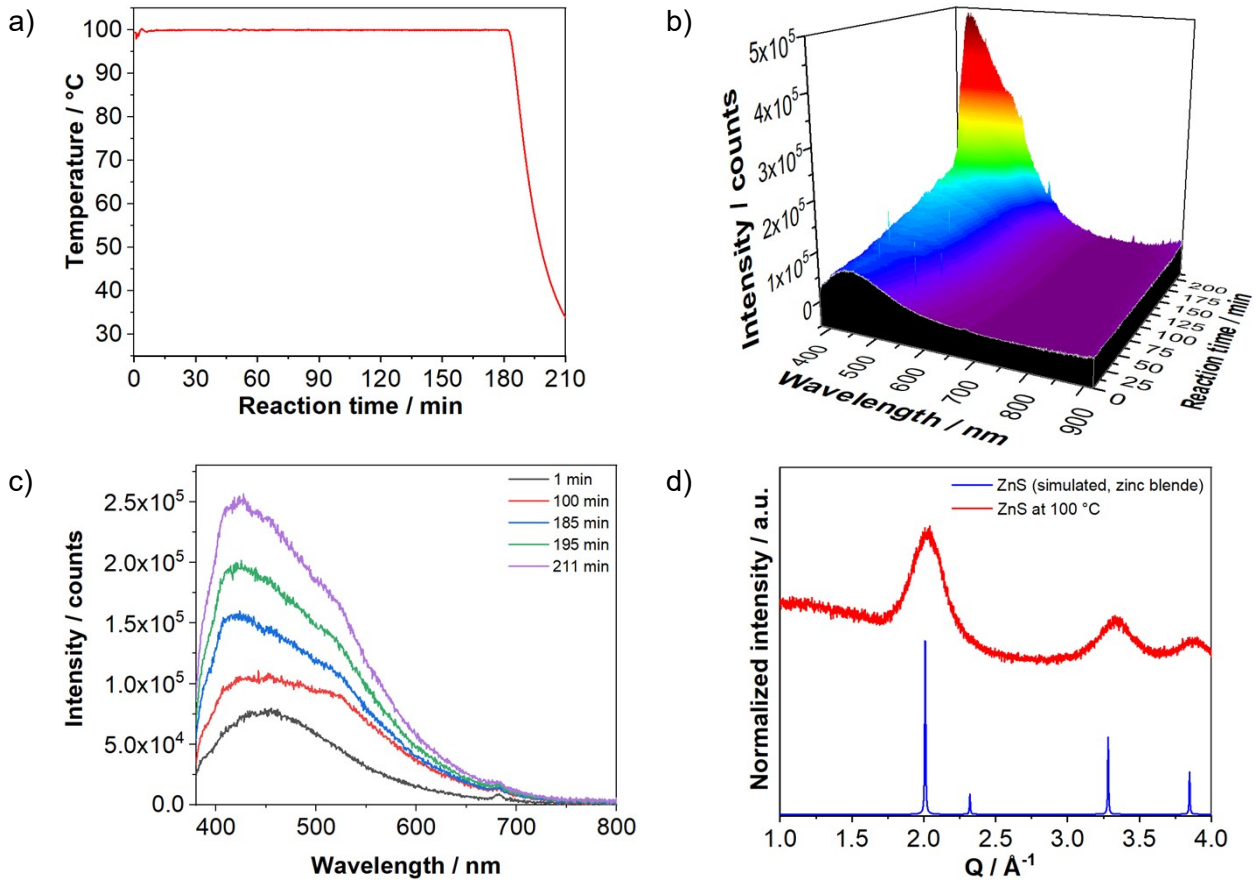

Figure S15: a) Time-dependent changes of the reaction temperature during the ZnS synthesis at 100 °C (Exps. XI and XII). b) and c) *In situ* luminescence spectra as well as d) respective *ex situ* XRD measurement of the product (Exp. XII) compared to the ZnS simulated [24] pattern.

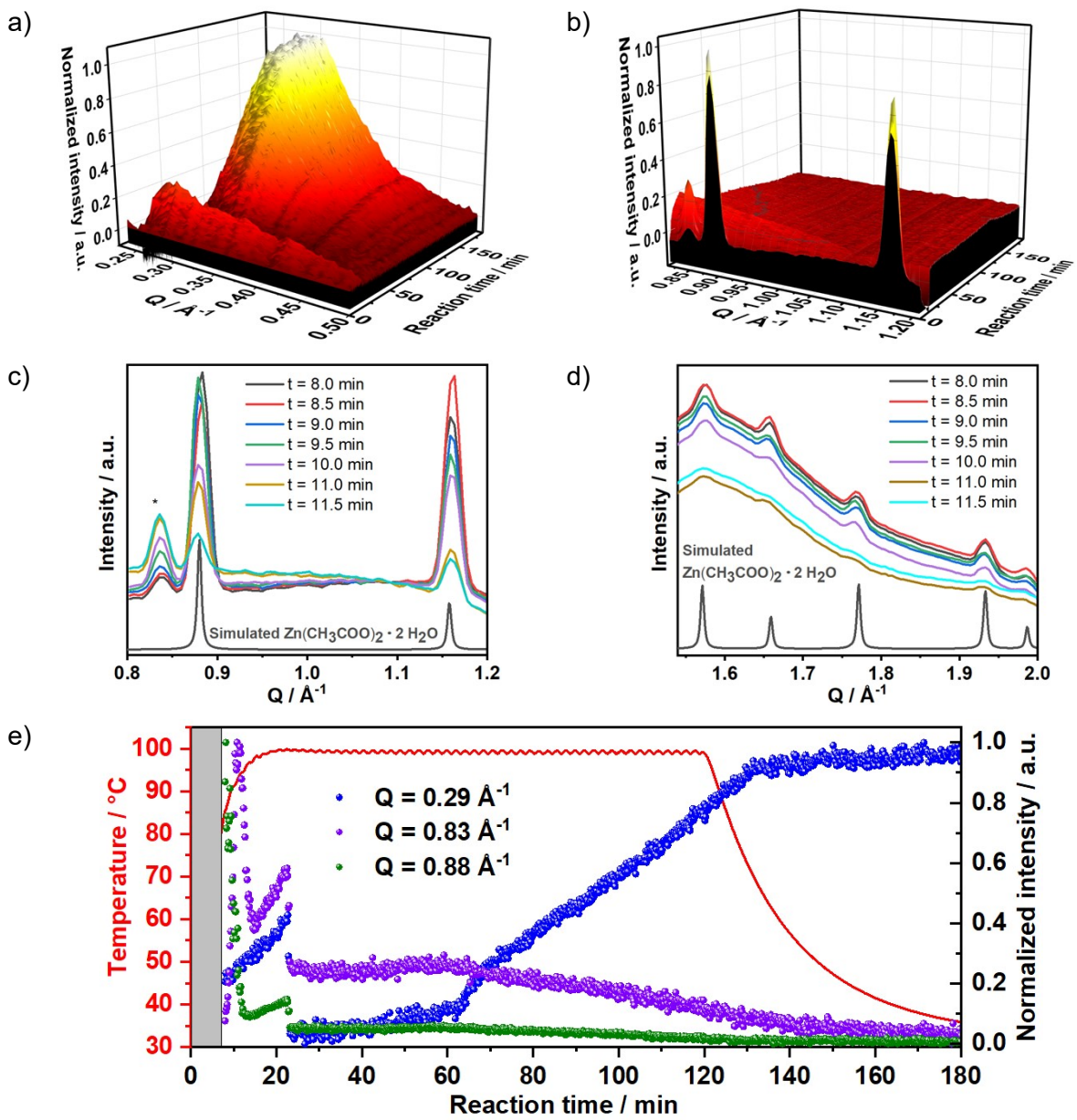

Figure S16: *In situ* XRD results recorded at the DESY P02.1 beamline during the reaction between $Zn(CH_3COO)_2 \cdot 2H_2O$ and thiourea in ethylene glycol at 100 °C (Exp. XIV). a) Increase of the background at the small angle range indicating the formation of nanoparticles. b)-d) Main reflexes assigned to $Zn(CH_3COO)_2$ and an unknown phase (*). e) Time-dependent profile of the temperature and reflexes at Q = 0.29 $Å^{-1}$ (NPs), Q = 0.83 $Å^{-1}$ (unknown phase) and Q = 0.88 $Å^{-1}$ $Zn(CH_3COO)_2 \cdot 2H_2O$.

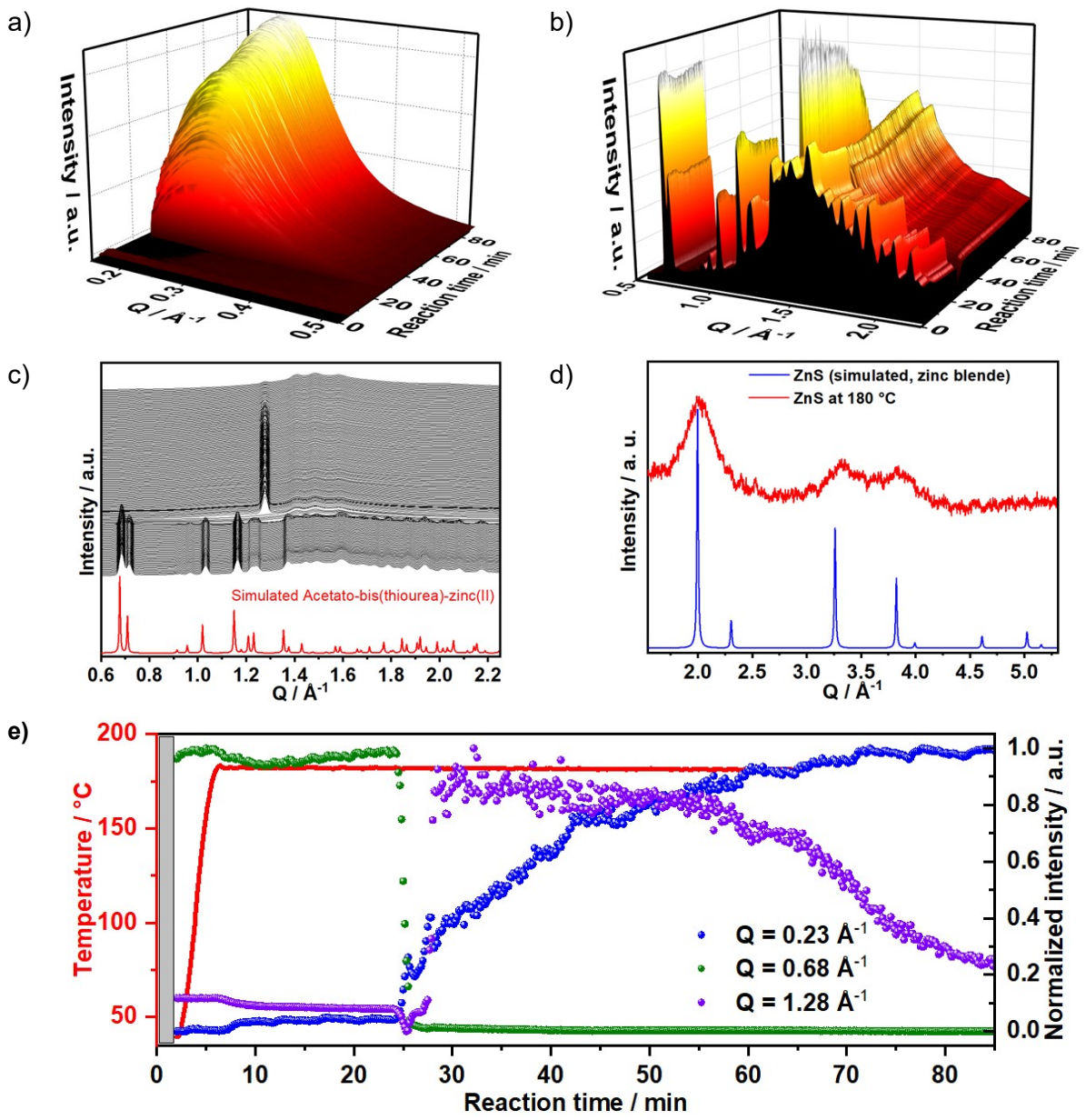

Figure S17: *In situ* XRD results recorded at the DESY P02.1 beamline during the reaction between $Zn(CH_3COO)_2 \cdot 2H_2O$ and thiourea in ethylene glycol at 180 °C (Exp. XV). a) Increase of the background at the small angle range indicating the formation of nanoparticles. b)-c) Main reflexes assigned to the acetato-bis(thiourea)-zinc(II) complex and an unknown phase. e) Time-dependent profile of the temperature and reflexes at Q = 0.23 Å^{-1} (NPs), Q = 0.68 Å^{-1} (acetato-bis(thiourea)-zinc(II) complex) and Q = 1.28 Å^{-1} (unknown phase).

7 References

[1] A. Schiener, A. Magerl, A. Krach, S. Seifert, H.-G. Steinrück, J. Zagorac, D. Zahn, R. Weihrich, *Nanoscale* **2015**, *7*, 11328–11333.

[2] C. Petit, P. Lixon, M. P. Pileni, *J. Phys. Chem.* **1990**, *94*, 1598–1603.

[3] L. Motte, C. Petit, L. Boulanger, P. Lixon, M. P. Pileni, *Langmuir* **1992**, *8*, 1049–1053.

[4] Y. Yin, X. Xu, X. Ge, C. Xia, Z. Zhang, *Chem. Commun.* **1998**, 1641–1642.

[5] B.-G. An, Y. W. Chang, H.-R. Kim, G. Lee, M.-J. Kang, J.-K. Park, J.-C. Pyun, *Sensor. Actuat. B-Chem.* **2015**, *221*, 884–890.

[6] C. Borriello, S. Masala, V. Bizzarro, G. Nenna, M. Re, E. Pesce, C. Minarini, T. Di Luccio, *J. Appl. Polym. Sci.* **2011**, *122*, 3624–3629.

[7] X. Tang, E. Kröger, A. Nielsen, S. Schneider, C. Strelow, A. Mews, T. Kipp, *Chem. Mater.* **2019**, *31*, 224–232.

[8] K. Boldt, N. Kirkwood, G. A. Beane, P. Mulvaney, *Chem. Mater.* **2013**, *25*, 4731–4738.

[9] X. Xie, Z. Zhang, Z. Chen, J. Wu, Z. Li, S. Zhong, H. Liu, Z. Xu, L. Zhilou, *Chem. Eng. J.* **2022**, *429*, 132115.

[10] J. H. Kim, J. G. Kim, J. Song, T.-S. Bae, K.-H. Kim, Y.-S. Lee, Y. Pang, K. H. Oh, H.-S. Chung, *Appl. Surf. Sci.* **2018**, 436, 556–561.

[11] F. Meneau, G. Sankar, N. Morgante, R. Winter, C. R. A. Catlow, G. N. Greaves, J. M. Thomas, *Faraday Discuss.* **2003**, *122*, 203-210.

[12] S. K. Shevell, “The Science of Color”, Elsevier Science, Amsterdam (2003).

[13] P. Lindenberg, L. R. Arana, L. K. Mahnke, P. Rönfeldt, N. Heidenreich, G. Doungmo, N. Guignot, R. Bean, H. N. Chapman, D. Dierksmeyer et al., *React. Chem. Eng.* **2019**, *4*, 1757–1767.

[14] H. Terraschke, M. Rothe, A.-M. Tsirigoni, P. Lindenberg, L. Ruiz Arana, N. Heidenreich, F. Bertram, M. Etter, *Inorg. Chem. Front.* **2017**, *4*, 1157–1165.

[15] N. Heidenreich, U. Rütt, M. Köppen, A. K. Inge, S. Beier, A.-C. Dippel, R. Suren, N. Stock, *Rev. Sci. Instrum.* **2017**, 88.

[16] P. Rönfeldt, E. S. Grape, A. K. Inge, D. V. Novikov, A. Khadiev, M. Etter, T. Rabe, J. Benecke, H. Terraschke, N. Stock, *Inorg. Chem.* **2020**.

[17] M. Krunks, J. Madarász, L. Hiltunen, R. Mannonen, E. Mellikov, L. Niinistö, *Acta Chem. Scand.* **1997**, *51*, 294–301.

[18] L. D. Nyamen, N. Revaprasadu, R. V.S.R. Pullabhotla, A. A. Nejo, P. T. Ndifon, M. A. Malik, P. O’Brien, *Polyhedron* **2013**, *56*, 62–70.

[19] A. S. Pereira, P. Tavares, P. Limão-Vieira, Radiation in Bioanalysis, 1, Springer Nature Switzerland AG, Cham, **2019**.

[20] F. Ulrich, W. H. Zachariasen, *Z. Kristallogr. Krist.* **1925**, *62*, 260–273.

[21] H. Sowa, *Solid State Sci.* **2005**, *7*, 73–78.

[22] T. Tkhanmanivong, V. M. Akimov, V. G. Andrianov, Y. T. Struchkov, A. K. Molodkin, *Russ. J. Inorg. Chem.* **1984**, *29*, 1033.

[23] B. Srinivasa Rao, B. Rajesh Kumar, V. Rajagopal Reddy, T. Subba Rao, *Chalcogenide Lett.* **2011**, *8*, 177–185.

[24] C.-Y. Yeh, Z. W. Lu, S. Froyen, A. Zunger, *Phys. Rev. B* **1992**, *46*, 10086–10097